Heliyon 9 (2023) e18353

Contents lists available at ScienceDirect

Heliyon

journal homepage: www.cell.com/heliyon

1-Butyl-3-methylimidazolium methane sulfonate ionic liquid corrosion inhibitor for mild steel alloy: Experimental, optimization and theoretical studies

Daniel Iheanacho Udunwa [a,b,***], Okechukwu Dominic Onukwuli [b,**], Mathew Chukwudi Menkiti [b], Valentine Chikaodili Anadebe [c,d,e,*], Maduabuchi Arinzechukwu Chidiebere [f]

[a] Department of Polymer and Textile Engineering, Federal University of Technology, Owerri, Imo State, Nigeria
[b] Department of Chemical Engineering, Nnamdi Azikiwe University, Awka, Anambra State, Nigeria
[c] Corrosion and Materials Protection Division, CSIR-Central Electrochemical Research Institute, Karaikudi 630003, Tami Nadu, India
[d] Academy of Scientific and Innovative Research (AcSIR), Ghaziabad 201002, India
[e] Department of Chemical Engineering, Alex Ekwueme Federal University, Ndufu Alike, P.M.B. 1010, Abakaliki, Ebonyi State, Nigeria
[f] Department of Science Laboratory Technology, Federal University of Technology, Owerri, Imo State, Nigeria

ARTICLE INFO

Keywords:
Ionic liquid
Acid corrosion
Mild steel
Electrochemical
MD-Simulation

ABSTRACT

The current research reports the performance of 1-butyl-3-methylimidazolium methane sulfonate ([C_4MIM][OMs](IL)) as effective corrosion inhibitor for mild steel in 1 M H_2SO_4 electrolyte. For proper evaluation, weight loss, electrochemical study, theoretical modeling and optimization techniques were used. Weight loss and electrochemical methods shows that the inhibition performance of [C_4MIM][OMs] on the metal surface strengthens as the concentration increases. Maximum inhibition efficiency of 85.71%, 92.5% and 91.1% at 0.8 g L^{-1} concentration of [C_4MIM][OMs] were obtained from the weight loss, polarization and impedance studies, respectively. In addition, response surface methodology (RSM) a statistical tool was used for modeling and optimization of the empirical data. The RSM model validates the empirical findings. Also, DFT/MD-simulation investigations evidenced that [C_4MIM][OMs] forms a barrier film on the mild steel surface. The result shows that the synthesized [C_4MIM][OMs] could open up opportunities in corrosion and materials protection for sustainability.

1. Introduction

The use of metals and alloys in chemical, construction, petrochemicals and automobile industry has been on the increase due to technological advancement. Metal corrosion becomes a significant industrial issue because it results in significant financial loss as a

* Corresponding author. Corrosion and Materials Protection Division, CSIR-Central Electrochemical Research Institute, Karaikudi 630003, Tami Nadu, India.
** Corresponding author. Department of Chemical Engineering, Nnamdi Azikiwe University, Awka, Anambra State, Nigeria.
*** Corresponding author. Department of Polymer and Textile Engineering, Federal University of Technology, Owerri, Imo State, Nigeria.
E-mail addresses: daniel.udunwa@futo.edu.ng (D.I. Udunwa), od.onukwuli@unizik.edu.ng (O.D. Onukwuli), anadebechika@gmail.com (V.C. Anadebe).

https://doi.org/10.1016/j.heliyon.2023.e18353
Received 12 April 2023; Received in revised form 7 July 2023; Accepted 14 July 2023
Available online 14 July 2023

result of exposure to aggressive solutions [1–4]. When expose to some operating conditions like high humidity, pH variation, and temperature, mild steel typically exhibits poor corrosion resistance [5,6]. The detrimental effects of metal degradation can be regarded as the major source of equipment failure and engineering impairment which causes sudden shutdown and poor production output [7, 8]. The degradation of a metal's surface as a result of environmental interaction is known as corrosion [9]. Various methods have been adopted to control corrosion, such as the use of chemicals as corrosion inhibitors, surface coatings, cathodic and anodic protection to combat the high risk and hazardous effects of corrosion [10–13]. Thus, using corrosion inhibitors during the industrial pickling process is one of the most effective approach.

Corrosion inhibitors are compounds that are intermittently introduced into the working fluid in small dose and adsorbed onto the metal surface *via* chemical, mechanical, or both to prevent further surface dissolution and corrosion [14,15]. The use of corrosion inhibitors has a distinct feature of not interfering with ongoing industrial operations. Corrosion inhibitors are used in many industries, including oil and gas exploration and production, water treatment plants, and fertilizer plants [16,17]. However, the application of some chemical based corrosion inhibitors have been limited as a result of their toxicity and immunological effect when exposed to the body [18,19]. In addition, majority of these synthetic or imported chemicals are scarce, requires complex synthesis route and very expensive to procure [20]. Nevertheless, many organic compounds having heteroatoms such as phosphorous, oxygen, nitrogen, and sulfur has been recognized to be potential replacement to the toxic corrosion inhibitors [21]. According to science, the most essential features for considering corrosion inhibitors are electron density, molecular structure, hydrophilicity, hydrophobicity, and dispersibility [22–24]. Due to the high electron density and basicity, corrosion inhibitors are mostly organic molecules containing heteroatoms and the advent of ionic liquid as a corrosion inhibitor is a desirable development.

Ionic liquid (ILs) are molten salts made up of organic cations and different anions. Ionic liquid base inhibitors have received significant attention in the area of corrosion control due to their unique features like low melting temperature, good solvation, negligible vapor pressure, high electrical conductivity, good thermal stability, non-toxic, availability and biodegradability [25]. These attributes portrays ionic liquids as a good corrosion inhibitor for metals in different aggressive environment, thus reducing the cost of equipment repair and importation of commercial inhibitors [26,27]. In view of the above highlights, some research works have been carried out with positive outcome in the area of metal protection. A novel tri-cationic surfactant based ionic liquid containing three quaternized nitrogen atoms was studied by Ref. [28]. The inhibition efficiency obtained at 5 mg/L concentration was above 90%, showing that the anti-corrosion effect of the synthesized surfactant on the metal surface even at low inhibitor concentration. Also, a novel bromide–cucurbit (7) uril supramolecular ionic liquid as a green corrosion inhibitor for the oil and gas industry was studied by Ref. [29]. Its inhibition efficiency was 97.54% at 100 mg/L/0.06 mM, and it was more stable at high temperature (333 K). Similarly, imidazolinium cation and 4–hydroxycinnamate anion ionic liquids as corrosion inhibitor for mild steel in 0.01 M NaCl alkaline solution was tested by Ref. [30]. It was found that the inhibitors were anodic in nature and adsorbed on the steel surface by physical and chemical methods. A new type of imidazole–based ionic liquids as corrosion inhibitor for steel in cement pore solution was investigated by Ref. [31]. These ionic liquids were mixed-type inhibitors, and the π–electrons in the benzoyl rings were attributed to the good inhibition performance of the studied ionic liquid. Also, the influence of imidazole-based ionic liquid as electrolyte additive on the performance of alkaline air Al- battery was investigated by Ref. [32]. The inhibition efficiency observed was 58.2% when the concentration of HMIC was 7 mM, and the anode utilization increased to 82.9%. Hence, from the above highlights, ionic liquid has been proven to be effective corrosion inhibitor owing to their molecular structure, biocompatibility, availability and environmental friendliness. Also, a comparative analysis of previous works with the current research is presented in Table 1.

Furthermore, in the quest for predicting the optimum conditions that necessitate the inhibition efficiency, response surface methodology (RSM) was employed as a statistical tool. Response surface methodology is a model equation used in solving complex, quadratic and nonlinear engineering problems. Many researchers have found these tool as a unique algorithm to evaluate the interactive effects between an input and output variables [41].

Table 1
Reports on ionic liquid as corrosion inhibitor in different corrosive environments.

Ionic liquid (IL) compound	Metal	Media	IE (%)	Maximum conc.	Inhibitor type	Reference
2-amino-4,5-imidazoledicarboxamide	Aluminum	1 M HCl	94.50	0.005 M	Cathodic-type	[33]
1-butyl-3-methylimidazolium thiocyanate	Aluminum 6061 Alloy	1 M HCl	98.20	3.00 Mm	Mixed- type	[34]
Two trimeric cationic imidazolium salts (APMI and APBI)	N80 steel	Oil field water	86.79 and 90.47	200 ppm	Mixed-type	[35]
L-histidine based	Mild steel	1 M HCl	98.80	2.00 Mm	Mixed-type	[36]
Isostearyl ethylimidonium ethosulfate [Quaternium-32]	Mild steel	0.013 M Ca $(OH)_2$	94.00	20 μmol^{-1}	–	[37]
1-methyl-3-propylimidazolium iodide	Mild steel	1 M H_2SO_4	91.00	1000 ppm	Mixed-type	[38]
1,3-bis [2-(4-Methoxyphenyl)-2-oxoethyl]-1H-ol-3-ium bromide	Al-15 6061	0.1 M HCl and 0.1 M H_2SO_4	98.30 and 98.80	0.05 mM and 0.5 Mm	Mixed-type	[39]
1-butyl-1-methylpyrrolidinium trifluoromethylsulfonate	Mild steel	3.5% NaCl	80.00	100 ppm	Cathodic-type	[40]
1-butyl-3-methylimidazolium methane sulfonate	Mild steel	1 M H_2SO_4	92.50	0.8 g L^{-1}	Mixed-type	Present

Hence, the novelties in this study work are as follows: (i) 1-Butyl-3-methylimidazolium methane sulfonate ionic liquid was synthesized as shown in Scheme 1 (ii) the inhibition performance of [C_4MIM][OMs] for mild steel in 1 M H_2SO_4 was evaluated; and (iii) the inhibitory action of the ionic liquid on the Fe surface was theoretically and empirically studied, and finally (iv) the interactive effects between the operating conditions and the expected response was predicted *via* RSM.

2. Experimental

2.1. Materials and metal preparation

Ethanol (CH_3CH_2OH) 96.8%, Acetone (CH_3COCH_3), 96.4%, *n*-methylimidazole, 1-butyl methyl sulfonate were purchased from Sigma-Aldrich. Mild steel composition is as follows: Mn (0.14%), P (0.23%), Si (0.04%), S (0.11%), C (0.25%), Cr (0.03%), Ni (0.08%), and Fe (99.12%). Prior to experiment, the specimen was cut into 4 cm × 3 cm x 0.1 cm, polished with emery papers (180, 200 and 1200 grits size). The impurities on the specimen was removed with acetone, rinsed with distilled water and dried in warm air. This is in line with the conventional method already reported [42].

2.2. Ionic liquid synthesis/characterization and surface analysis

1-butyl-3-methylimidazolium methane sulfonate was prepared by mixing 0.60 g of *n*-methylimidazole (Sigma Aldrich, St. Louis, USA) and 1.8 g 1-butyl-methanesulfonate (Sigma Aldrich, St Louis, USA) simultaneously inside a 250 ml tumbler and stirred for 30 min. The stirred mixture was put in a microwave and radiated for 8 min using 1-butyl-3-methylimidazolium tetrafluoroborate [bmim][BF_4] as a catalyst at temperature of 110–115 °C [43]. The product was collected, washed four times and dehumidified using ethyl acetate. [C_4MIM][OMs] was obtained and the yield was 96.10% and melting point in the range of 71–73 °C. All chemicals employed were of analytical grade and were used without further purification.

In order to have an insight on the structural characteristics of [C_4MIM][OMs] molecules before and after corrosion, infrared spectroscopy (FT-IR) was performed using PerkinElmer 100 F T-IR spectrophotometer meter for the pure and after corrosion inhibition (5hr immersion). The FTIR analysis was performed within the wavelength of 400–4000 cm^{-2}. Furthermore, SEM/AFM analysis of corroded and inhibited metal surfaces after 5hr was performed using scanning electron microscope (model-JEOL-JSM-6390) Czech Republic. Also, atomic mass spectroscopy was performed using Pipcoplus 2500 to successfully inspect the surface roughness of the corroded and inhibited metal surface [44].

2.3. Mass loss analysis

Mass loss experiment was performed at temperatures 303–343 K to accurately evaluate the mass loss, corrosion rate (*CR*) and inhibition efficiency (*IE*). The polished mild steel was measured using a weighing balance. The first weight of the coupon was recorded. Subsequently, mild steel coupon was immersed into the test solution (1 M H_2SO_4). The mild steel coupon was removed after corrosion test at varying time. The mild steel coupon was washed with acetone and rinsed with distilled water to remove external deposits and later dried in warm air. Similar procedure was performed using varying concentration of [C_4MIM][OMs]. In each case, weight loss was evaluated as the difference between the initial weight of the steel and after corrosion test in acidic medium. The values were used to calculate the *CR* and *IE* according to Eqs. (1)–(3) [45,46].

$$\Delta w = w_i - w_f \tag{1}$$

$$CR = \frac{w_{bl} - w_{inh}}{A(m^2) \times (t)day} \tag{2}$$

$$\mathrm{IE\%} = \frac{\mathrm{w_{bl}} - \mathrm{w_{inh}}}{\mathrm{w_{bl}}} \times 100 \tag{3}$$

Where w_i and w_f denote initial and final weight of mild steel specimen, respectively; w_{bl} and w_{inh} denote loss in weight in the absence of

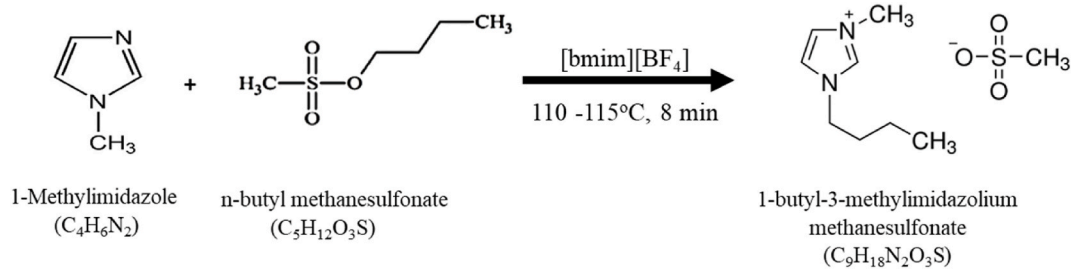

Scheme 1. Synthesis route and chemical composition of [C_4MIM][OMs].

inhibitor and loss in weight in the presence of inhibitor, respectively. A (m^2) represents the area of the metal and (t) depicts the immersion time. The surface coverage (θ) was determined using Eq. (4) [47].

$$\theta = \frac{W_{bl} - W_{inh}}{W_{bl}} \tag{4}$$

2.4. Electrochemical analysis

The electrochemical set up used in this investigation consists of VERSA-STAT 400 full set of DC voltammetry and a Potentio/Galvonstat with E-chem software. Three sets of electrodes were used. The three-electrodes employed were mild steel used as working electrode having the surface exposed by 1 cm × 1 cm in area (cm^2), standard platinum foil as counter electrode, and a saturated calomel electrode used as the reference electrode [48]. Electrochemical impedance spectroscopy (EIS) investigation was performed using a potential of 5 mV at a frequency sweep of 1000 kHz–100 kHz. Tafel polarization test was performed at a potential range of −200mV to +200 mV versus OCP at a scan rate of 0.5 mV s^{-1}. The anodic and the cathodic graphs of the Tafel plots were marked out to obtain the corrosion current densities (i_{corr}). For an accurate reproducibility of acquired results, the mean value of duplicate experiments was presented. Eqs. (5) and (6) were employed to calculate the inhibition efficiencies [49].

$$IE\% = \left(\frac{i_{0_{corr}} - i_{corr}}{i_{0_{corr}}}\right) \times 100 \tag{5}$$

$$IE\% = \left(\frac{R_p^{inh} - R_p^o}{R_p^{inh}}\right) \times 100 \tag{6}$$

where $i_{0_{corr}}$, and i_{corr}, signify corrosion current density in the blank and corrosion current density in the presence of inhibitor. R_p^{inh} and R_p^o denote polarization resistance in the presence of [C_4MIM][OMs] and polarization resistance in the blank, respectively.

2.5. Theoretical modeling

Quantum chemical calculation was performed using BIOVIA material studio 7.0. The density functional theory (DFT) assemble system $DMOL^3$ was employed for the simulation of [C_4MIM][OMs] ionic liquid and mild steel surface interaction. Electronic variables employed comprises of an unrestricted spin polarization using dual numerical plus (DNP) base set 3.5 and perdew-wang (PW) local relation density functional. Fe (110) was considered as the slab for the simulations. Imported Fe (110) surface was magnified to a 12× 10 super cell and calculations were performed in the super cell using a compass force field (COMPASS) and the smart computation using NVT canonical ensemble.

2.6. Statistical analysis

Response surface methodology (RSM) is a statistical tool used for design and optimization process. RSM is capable of analyzing the interactive effects (input and output variables) existing within a system thereby predicting the optimum conditions. The prime factors considered as inputs are inhibitor concentration (A), temperature (B) and time (C), while the output is denoted as inhibition efficiency (IE %) [50]. The regression model associated with the RSM is presented in Eq. (7).

Table 2
Effect of process variables (time, temperature, inhibitor conc.) and their reaction.

Time (hr)	ω_o (g)	CR_o (mg/cm hr)	ω_1 (g)	CR1 (mg/cm hr)	IE (%)	θ
1.0	0.16	13.333	0.06	5.000	62.50	0.6250
2.0	0.37	15.417	0.07	2.917	81.08	0.8108
3.0	0.56	15.556	0.08	2.222	85.71	0.8571
4.0	0.58	12.083	0.11	2.292	81.03	0.8103
5.0	0.60	10.000	0.12	2.000	80.00	0.8000
Effect of temperature (K)						
303	0.52	14.444	0.12	3.333	76.92	0.7692
313	0.56	15.556	0.08	2.222	85.71	0.8571
323	0.57	15.833	0.09	2.500	84.21	0.8421
333	0.63	17.500	0.20	5.556	68.25	0.6825
343	0.65	18.056	0.22	6.111	66.15	0.6615
Effect of IL concentration						
0.00	0.56	15.556	–	–	–	–
0.20			0.24	6.667	57.14	0.5714
0.40			0.18	0.500	67.86	0.6786
0.60			0.13	3.611	79.79	0.7979
0.80			0.08	2.222	85.71	0.8571
1.00			0.10	2.778	82.14	0.8214

$$Y = Z_o + Z_{1X1} + Z_{2X2} + Z_{3X3} + Z_{12X1X2} + Z_{13X1X3} + Z_{23X2X3} + Z_{11X1^2} + Z_{22X2^2} + Z_{33X3^2} \quad (7)$$

Y is the output (response prediction), representing the IE (%), Z_o is the constant parameter, Z_1, Z_2 and Z_3 are linear terms, Z_{12}, Z_{13} are product terms, Z_{11}, Z_{22} and Z_{33} are the quadratic terms. X_i is taken to be coded factor (MI) normally programmed in levels of (0, −1, and +1). From the 20 runs of experiment, design expert program was used to evaluate the analysis of variance (ANOVA) that was utilized to analyze the design significance and predict the response (inhibition efficiency).

3. Result and discussion

3.1. Weight loss evaluation

Despite time-consuming approach of mass loss method in predicting corrosion rate and the inhibition assessment, it has remained more reliable way of obtaining accurate data. Table 2 displays the gravimetric results for steel in blank 1 M H_2SO_4 solution and in presence of [C_4MIM][OMs] at varying concentrations at varying time. As evidenced, addition of more dosage of [C_4MIM][OMs] into the 1 M H_2SO_4 solution expedites the anti-corrosion ability of [C_4MIM][OMs]. Also, accompanied by regular increase in [C_4MIM][OMs] concentration and time, corrosion rate decreases, while surface coverage increases which is evidenced by the virtue of the inhibitor molecules to shield the steel surface from dissolution [51]. These behavior shows that the anti-corrosion ability of [C_4MIM][OMs] increases with respect to inhibitor concentration and time as shown in Table 2. As evidenced in Table 2 inhibition efficiency of 85.71% prevailed at 0.8 g L^{-1} of [C_4MIM][OMs]. The inhibition performance of [C_4MIM][OMs] is due to the heteroatoms and dispersibility of the ionic liquid molecule on the metal surface which give rise to large inhibitor molecule coverage. However, highest inhibition efficiency was attained at 3 h and temperature of 313 K. The observe trend is due to less acquisition of energy influence that may cause desorption of ionic liquid molecules from the metal surface at the initial stage of inhibitor adsorption and at medium temperatures. At high temperatures, dissolution of mild steel is enhanced, therefore the value of the inhibition efficiency tends to decrease appreciably. This phenomenon is attributed to the severe acquisition of energy within the system which affect the corrosive solution and consequently results to instability and desorption of ionic liquid molecules from the mild steel surface within the temperatures of 333–343 K [52].

3.2. Inhibitor characterization via FTIR, and surface analysis (SEM/AFM)

Fourier transform infrared spectroscopy (FTIR) is an analytical tool used to identify the presence and nature of functional groups in a compound [53]. FTIR technique was used in this present study to elucidate further on the functional group present in the pure ionic liquid and that of after corrosion inhibition study as shown in Fig. 1a–b. Fig. 1a revealed the presence of peak number 1043.7–1151.7 cm^{-1} assign to *C*–O, nitro peak number 1283.6 cm^{-1} assign to *N*–O, nitrile peak number 1401.5 cm^{-1} assign to *C*–N, acid anhydrite peak number 1625.1–2173.0 cm^{-1} assign to C=O, aldehyde peak number 2974.4 cm^{-1} assign to *C*–H, amine/alcohol peak number 3399.9 cm^{-1} assign to *N*–H/O–H groups which can be ascribed as their functional groups. Furthermore, Fig. 1b shows a significant effect of [C_4MIM][OMs] at 0.8 g L^{-1} on the mild steel surface in 1 M H_2SO_4 solution after immersion for maximum period of 5hr. Close examination of the FTIR spectra after corrosion inhibition reveals appreciable change in the peaks and intensities [54]. In addition, Fig. 1b revealed fewer peaks that corresponds to *C*–O, C=O and *O*–H and their peak order are 1084.7 cm^{-1}, 1636.3 cm^{-1} and 3339.7 cm^{-1}, respectively. Stretched *C*–O at 1043.7–1151.7 cm^{-1} shifted to *C*–O at 1084.7 cm^{-1}. Stretched C=O at 1625.1–2173.0 cm^{-1} shifted to C=O at 1636.3 cm^{-1} and stretched *O*–H at 3399.9 cm^{-1} adjusted to 3339.7 cm^{-1}. More so, one can attribute it to the synergistic performance of the functional groups of [C_4MIM][OMs] molecules to bind with Fe^{2+} from the mild steel surface that resulted in the formation of [C_4MIM][OMs]/Fe^{2+} complexes [31].

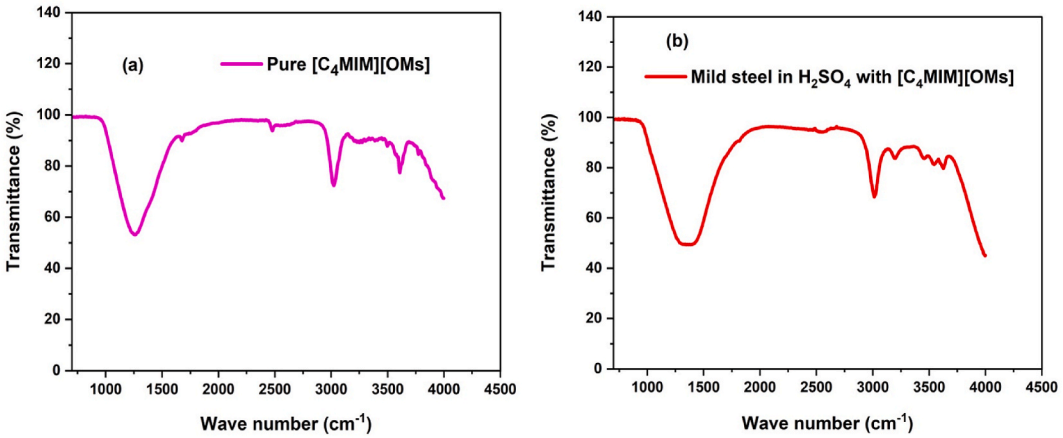

Fig. 1. (a) FTIR analysis of [C_4MIM][OMs]; (b) adsorbed [C_4MIM][OMs] molecule.

Also, atomic force microscopy (AFM) in addition with scanning electron microscopy (SEM) were used to analyze the surface morphology of blank and inhibited metal surfaces immersed in 1 M H_2SO_4 solution for 5hr at optimum inhibitor concentration of 0.8 g/L as shown in Fig. 2. As evidenced, in the absence of the inhibitor, Fig. 2a shows a mountain like deposits with dark pits owing to the acid penetration to the steel surface, while Fig. 2b exhibited plane surface due to better surface coverage owing to the ionic liquid adsorption. As a result, the mean surface crack of the steel was successively reduced owing to the attachment of the inhibitor molecule on the steel surface. Fig. 2c-d presents the SEM result that depicts corroded mild steel by the acid solution. Corrosion cracks and pits were visible because of the acid penetration to the mild steel. Conversely, Fig. 2d portrays a smooth surface which was protected by [C_4MIM][OMs]. This is attributed to decrease in attack due to the addition of [C_4MIM][OMs] molecules in the environment that retards the action of corroding moieties. The corrosion inhibition of [C_4MIM][OMs] is enhanced by increasing the concentration which promotes efficient surface coverage and rapid bonding of inhibitor molecules on the metal surface [4].

3.3. Isotherm study

It is important to study the kinetics involved in the interaction of mild steel in acidic solution (blank) and inhibited solution [55]. When a metal is dipped into an electrolyte, oxidation of the metal to some intermediate state occurs. The charge distribution relies on the effects of steel, nature of corrosive media, coupled with the degree of solubility of negative ions in water [56]. The procedure associated with mild steel dipped in 1 M H_2SO_4 in the presence of [C_4MIM][OMs] is mostly investigated using the adsorption isotherm [57]. In this regard, adsorption isotherms including the Temkin, Frumkin, Langmuir and Flory-Huggins isotherms were tested using data obtained from the experiment at 313 and 323 K, and the Langmuir isotherm model gave best fit as shown in Fig. 3. As displayed in Fig. 3, a linear graph accompanied by a relationship coefficient (R^2) of 0.9953 and 0.9880 was obtained at 313 and 323 K. These findings confirm that the surface of [C_4MIM][OMs] molecules on the mild steel surface conform to Langmuir adsorption isotherm in accordance with Eq. (8) [58,59].

$$\frac{C}{\theta} = \frac{1}{K_e} + C \tag{8}$$

where the C represents inhibitor concentration in (gL^{-1}), θ is surface coverage of corroding mild steel and K_e denote the equilibrium constant for [C_4MIM][OMs]/mild steel interface. The Gibb's free energy (ΔG_{ads}) was computed from Langmuir isotherm parameters using Eq. (9) [60,61].

$$\Delta G_{ads} = -RT\ In\ (55.5K_e) \tag{9}$$

where R denotes molar gas constant of value 8.3142 J K^{-1} mol^{-1}, T indicates gas temperature, K_e denotes the coefficient of adsorption

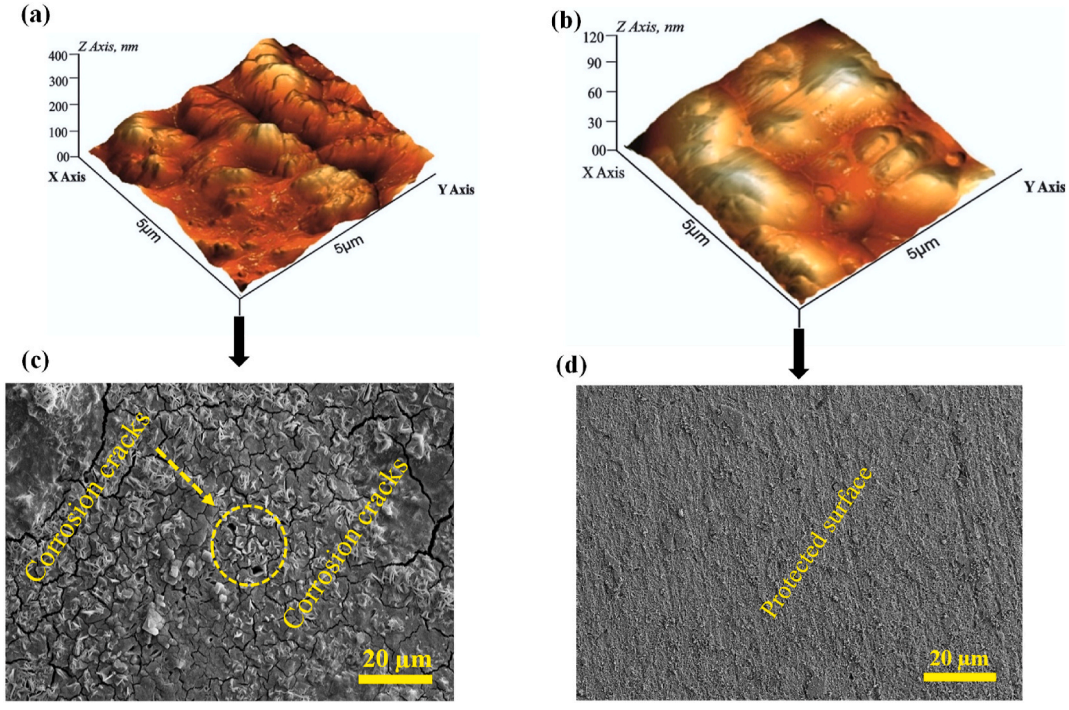

Fig. 2. (a) AFM image of MS in 1 M H_2SO_4 without and (b) with 0.8 g/L of [C_4MIM][OMs], (c) SEM image of MS in blank; (d) in presence of 0.8 g/L of [C_4MIM][OMs] for 5 h.

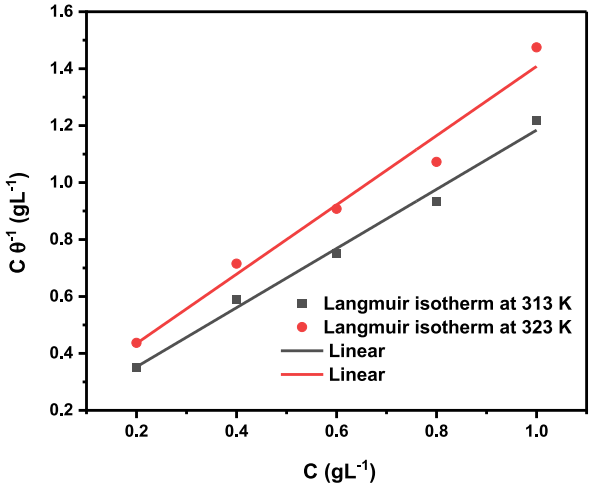

Fig. 3. Langmuir isotherm plot for $[C_4MIM][OMs]$ in 1 M H_2SO_4 solution at 313 and 323 K.

and 55.5 signifies molar concentration of water fragments contained in 1 L acid solution. Computed values of K_e and ΔG_{ads} obtained from interaction of $[C_4MIM][OMs]$ on mild steel surface are shown in Table 3. The associated negative values of ΔG_{ads} corroborates that the adsorption mechanism is spontaneous. Basically, a value of ΔG_{ads} approaching -20 kJ mol^{-1} stand for physisorption mechanism, while the value close to -40 kJ mol^{-1} or higher negative values signifies chemisorption mode [62]. In this study, the observed ΔG_{ads} values were less than -40 kJ mol^{-1} which strongly suggest that the mild steel surface is totally covered by $[C_4MIM][OMs]$ molecules *via* physical process. This process of physical adsorption produced the desired barrier that prevented the mild steel from degradation in the acid medium [59].

3.4. Temperature effect and activation parameters

Change of temperature and activation energy on mild steel corrosion in 1 M H_2SO_4 was examined by appraising corrosion rate at temperature of 313 and 323 K. Table 4 demonstrated that favorable inhibition efficiency of $[C_4MIM][OMs]$ molecules is accomplished at medium temperature range of 313 K and the IE % decreases as the temperature increases. This stipulates that corrosion inhibition of $[C_4MIM][OMs]$ was determined by temperature effect. Herein, increase in temperature weakens the bonding between $[C_4MIM][OMs]$ molecules and that of metal surface thereby reducing the surface coverage and leaving the steel surface vulnerable to corrosion damage [63,64]. In other to examine the relationship between heat, temperature, and energy change within the system, thermodynamic parameters were considered. Arrhenius equation was used to scrutinize temperature dependent of the *CR*. The Arrhenius Equation is stated in Eq. (10).

$$logCR = logA - \frac{E_a}{RT} \tag{10}$$

Where, R denotes gas constant equal to 8.3142 mol^{-1} K^{-1}, T signifies Kelvin temperature, E_a mean activation energy and A stand for Pre exponential component, respectively. The change of the logarithm of corrosion rate with the inverse of temperature for mild steel dissolution is presented in Fig. 4 while, Table 5 shows calculated thermodynamic variables from the Arrhenius model. It is worthy to note that the obtained value of the activation energy was positive and greater than the one for the blank solution, this suggest that the performance of $[C_4MIM][OMs]$ increases with concentration and that activation energy of the system containing an inhibitor will be higher compared with the activation energy of blank system [62]. In this regard the dissolution of mild steel in 1 M H_2SO_4 is slower with addition of $[C_4MIM][OMs]$ and occurs *via* physical adsorption mechanism while, the reverse process is chemisorption [65]. To evaluate other thermodynamic parameters such as the enthalpy of activation (ΔH_a) and entropy of activation (ΔS) the transition state Eq. (11) was employed.

$$CR = \frac{RT}{Nh}\, exp\left(\frac{\Delta S}{R}\right)\, exp\left(-\frac{\Delta H_a}{RT}\right) \tag{11}$$

Table 3
Langmuir parameters of $[C_4MIM][OMs]$ in 1 M H_2SO_4 electrolyte at 313 and 323 K.

Temperature (K)	K_e ($Lmol^{-1}$)	Slope	R^2	ΔG_{ads} ($kJmol^{-1}$)
313	225.44	1.0394	0.9953	−24.55
323	192.60	1.2166	0.9880	−24.90

Table 4
Variables obtained from gravimetric experiment for corrosion of MS in 1 M H_2SO_4.

Inhibitor conc. (gL^{-1})	*T* *(K)*	*CR* (mg cm^{-2} h) Table 5: Parameters obtained from mass loss experiment for mild steel immersed in $1H_2SO_4$ with out and with 0.8 g/L [C1MIM][OMs].	log (*CR*) (mg cm^{-2} h)	*1/T* (K^{-1}) X 10^{-3}	*IE* (%)
Blank	303	14.444	1.1597	3.3	–
	313	15.556	1.1919	3.2	–
	323	15.883	1.2009	3.1	–
	333	17.500	1.2430	3.0	–
	343	18.056	1.2566	2.9	–
With 0.8 g L^{-1} of [C4MIM][OMs]	303	3.333	0.5228	3.3	0.7692
	313	2.222	0.3467	3.2	0.8571
	323	2.500	0.3979	3.1	0.8421
	333	5.556	0.7447	3.0	0.6825
	343	6.111	0.7861	2.9	0.6615

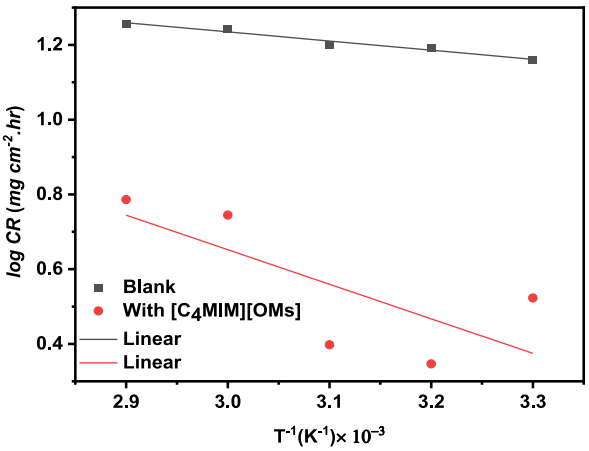

Fig. 4. Arrhenius graphs for mild steel corrosion in 1 M H_2SO_4.

Table 5
Thermodynamic parameters from Arrhenius plot for mild steel corrosion in 1 M H_2SO_4.

Inhibitor (gL^{-1})	Gradient (mg K cm^{-2}.h) $\times 10^{-3}$	R^2	Intercept	E_a ($kJmol^{-1}$)	ΔS ($(kJmol^{-1})$	ΔH_a ($kJmol^{-1}$)
Blank	−0.2449	−0.98353	1.9696	0.0049	−159.866	−4.689
With [C_4MIM][OMs]	−0.9246	−0.73466	3.4259	0.0177	−131.981	−17.704

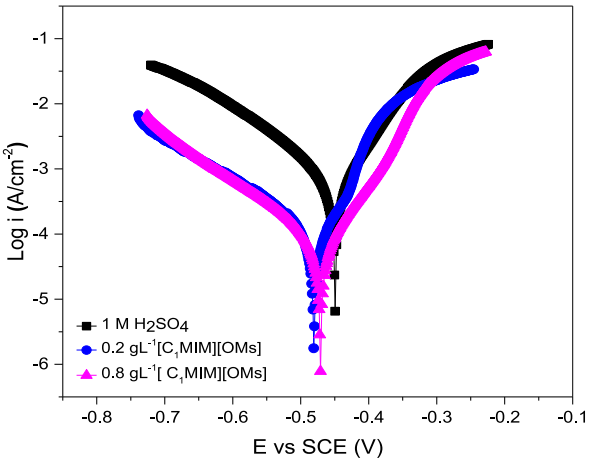

Fig. 5. Polarization curve for mild steel corrosion in blank 1 M H_2SO_4 and with [C_4MIM][OMs].

where ΔS signifies entropy of activation, ΔH_a denotes the enthalpy of activation, h stand for Planck's constant equal to 6.6261×10^{-34} and N denotes Avogadro's constant of value 6.023×10^{-23}, respectively. The gradient equal to $-\frac{\Delta H_a}{2.303R}$ and the intercept equivalent to $log\left(\frac{R}{Nh}\right) + \left(\frac{\Delta S}{2.303R}\right)$ deduced from the plot of log (CR/T) vs $1/T$ and were employed to evaluate worth of ΔS and ΔH_a, respectively [66]. The adsorption capability of [C_4MIM][OMs] molecules can be proven *via* substitution of water molecules by the ionic liquid ([C_4MIM][OMs]$_{(solution.)}$) on the Fe surface ($H_2O_{ads.}$) [65]. This action revealed that the cathonic molecule from the ionic liquid is bonded on the mild steel surface *via* electrostatic force and this action successfully protected the mild steel from further deterioration [66].

3.5. Electrochemical measurement

Potentiodynamic polarization curve for mild steel in blank and inhibited acid solution is presented in Fig. 5. The blank serves as the control. As evidenced, the addition of [C_4MIM][OMs] into the electrolyte reduces the effect of the corrosion current densities of the anodic and cathodic sides of the graph compared to the uninhibited solution. By this action, corrosion potential (E_{corr}) and corrosion current density (i_{corr}) shifted to a new value that stabilizes the system [32,67]. This phenomenon shows that [C4MIM][OMs] molecules obviously obstruct the mild steel corrosion in the acid environment. Close scrutiny of the Tafel polarization shows that [C_4MIM][OMs] molecules controlled both corrosion rate of the steel and hydrogen evolution [68]. At this moment the anodic (β_a) and cathodic (β_c) region were extrapolated. The corrosion current density (i_{corr}) and corrosion potential (E_{corr}) are shown in Table 6. The inhibition efficiency attained for the Tafel polarization analysis was 92.5% at 0.8 g L^{-1} inhibitor concentration. The potentiodynamic curves were less than 85 mV at maximum inhibitor concentration which establishes [C_4MIM][OMs] as a mixed-type inhibitor [8], but cathodic predominance [69].

Furthermore a non-destructive test *via* electrochemical impedance spectroscopy (EIS) approach was considered for mild steel dissolution in blank 1 M H_2SO_4 and inhibited solution as presented in Fig. 6. It shows the surface reactions occurring at the Fe solution/interface. Evidently, Fig. 6a, depicts the Nyquist plot for mild steel dissolution in 1 M H_2SO_4 and with varying [C_4MIM][OMs]. The blank solution was used as a control factor in comparing the inhibited results. The Nyquist plot evidenced a depressed semicircle for the blank and in the inhibited solutions with a double hump nature for the inhibited solutions [70]. However, the Nyquist plots obtained for the inhibited solutions exhibits high diameter compared to the blank sysytem. This observation demonstrates an intense charge transfer that enhances surface resistance of mild steel when the concentration of [C_4MIM][OMs] increases compared to the blank system [71]. This phenomenon indicates the presence of a barrier film layer on the mild steel surface which preserves the steel surface [72]. An increase in magnitude of the impedance spectra was observed from the electrolyte containing 0.8 g L^{-1} [C_4MIM][OMs] compared to the system having 0.2 g L^{-1} [C_4MIM][OMs]. In addition, phase plots and Log modulus plots revealed that the corrosion inhibition of [C_4MIM][OMs] was successively enhanced by the amount of [C_4MIM][OMs] added into the electrolyte as shown in Fig. 6b–c. This process is ascribed to even distribution of [C_4MIM][OMs] molecules on the mild steel imparting enough surface coverage that forms a barrier film obstructing the ingress of the corrodent [32]. The calculated worth of log/Z/enhanced significantly at low frequency with respect to [C_4MIM][OMs] concentration. The impedance variables were fitted into equivalent circuit (Fig. 6d) as previously reported in literature [49]. The circuit diagram is made up of electrolyte resistance (R_s), charge transfer resistance (R_{ct}) + inhibitor film resistance (R_f)), and CPE respectively. The CPE was employed to scrutinize and obtain a precise fit of the impedance data (Fig. 6d). The relationship correlating the CPE with the impedance of the system is given as Eq. (12) [48].

$$Z_{CPE} = Y_o^{-1}\left(j\omega_i^{-n}\right) \tag{12}$$

where, n and Y_o are the exponent and the *CPE*, respectively, $j^2 = -1$ represent the imaginary number, ω_i denotes angular frequency measured in $rads^{-1}$, when $n = -1$, is an inductor, if n is 0, it is a resistor and if n is 1, it is a capacitor [48,73]. The "n" value estimate the nature of the electrode surface with respect to blank and inhibited surfaces. The EIS data obtained are presented in Table 7.

3.6. DFT/MD-simulation approach

DFT is a simulation model developed to ascertain the correlation between experimental and theoretical data. The DFT gives a comprehensive information of the inhibitor film on the metal surface. Therefore, is quite fascinating researching on electron allocation in frontier molecular orbital (FMO), as to scrutinize the reactivity of the ionic liquid molecules. DFT was employed to determine the geometric configuration by the aid of $Dmol^3$ software (Biovia). The optimized structure of [C_4MIM][OMs] was realized employing the double numerical plus (DNP) base set. The optimized inhibitor molecule is shown in Fig. 7a. In addition, the active sites like the highest occupied molecular orbital (HOMO) and lowest unoccupied molecular orbital LUMO were studied [74].

Remarkably, the study of the HOMO and LUMO helped to have a recognition into the inhibition processes of the [C_4MIM][OMs] regarding Fe (110) plane concerning investigating the structure-reactivity relation. Fig. 7b–f shows the electron density, HOMO, and

Table 6
Polarization study for MS corrosion in 1 M H_2SO_4 in blank and with [C_4MIM][OMs].

Method	E_{cor} (mV vs SCE)	I_{corr} (μA cm^{-2})	β_a ($mvdec^{-1}$)	β_c ($mvdec^{-1}$)	IE (%)	θ
1 M H_2SO_4	−769.4	645.9	346.7	290.6	–	–
0.2 g L^{-1}	−745.3	70.4	286.4	265.7	89.1	0.891
0.8 g L^{-1}	−728.2	48.7	266.3	258.3	92.5	0.925

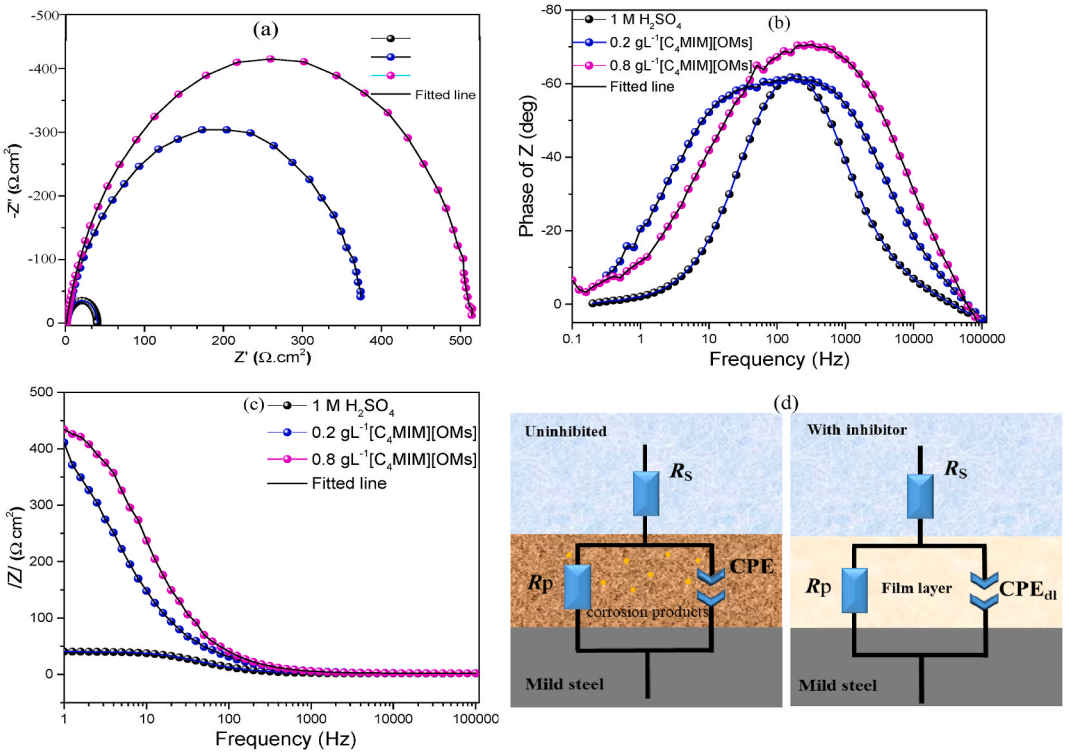

Fig. 6. (a) Nyquist (b) Phase angle (c) Log Modulus plot (d) equivalent circuit model for mild steel immersed in blank 1 M H_2SO_4 and in varying inhibitor concentration.

Table 7
Impedance variables for corrosion control study in 1 M H_2SO_4.

System	R_s (Ω cm)	R_p (Ω cm)	$Y_O(\times 10^{-9})\Omega^{-1}cm^{-1}$	n	$Cdl(\times 10^{-9})\mu Fcm^{-2}$	IE %
Blank	0.05	0.110	2.01	0.92	1.02	–
0.2 g L^{-1} [C_4MIM][OMs]]	0.07	0.793	7.26	0.93	2.56	86.1
0.8 g L^{-1} [C_4MIM][OMs]	0.09	1.236	4.03	0.93	2.50	91.1

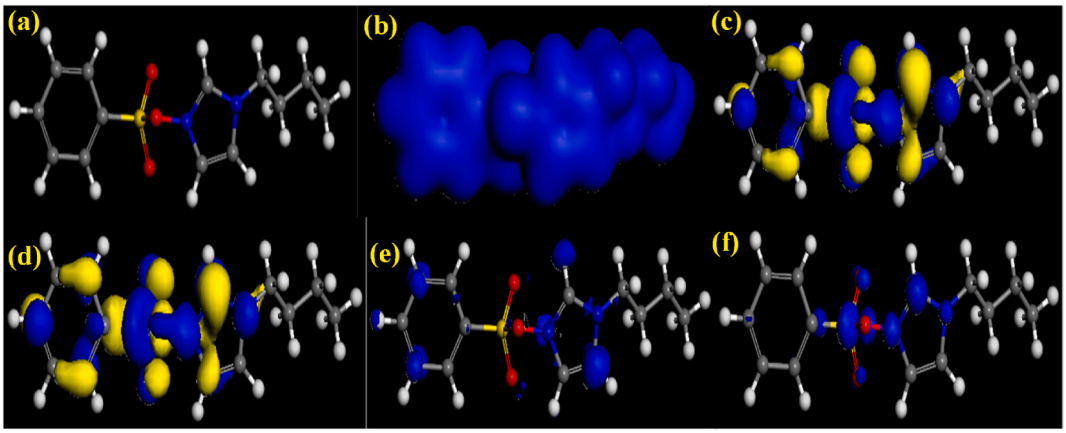

Fig. 7. DFT features of [C_4MIM][OMs] (a) Optimized structure (b) Electron density (c) HOMO (d) LUMO (e) Electrophilic (f) Nucleophilic. Atom legend: white = H; gray = C; red = O; blue = N and yellow = S.

LUMO distribution of [C_4MIM][OMs] molecules. As evidenced from Fig. 7c–d both HOMO and LUMO orbital distributions show significant divergence in the entire molecules. These outcomes demonstrate that [C_4MIM][OMs] molecules have mobile locations by virtue of which they can interact with the mild steel surface [75]. Also, the HOMO orbitals are frequently connected with the capability to donate electrons from inhibitor molecules to a relevant acceptor [76] which is accredited to the high value of E_{HOMO} (- 4.0640) energies compared to E_{LUMO} (−1.0085). The HOMO and LUMO distributions in the [C_4MIM][OMs] molecules are centralized inside the structure of nitrogen (N^+) atom and equally localizes inside oxygen (O^-) atom [27]. This shows that the chemical reactiveness of [C_4MIM][OMs] molecules with Fe (110) plane will probably occur through the portion of [C_4MIM][OMs] structure comprising nitrogen and oxygen particles like C=N, *C*–O, *C*–N, *N*–N, *C*–O and the π-electrons [76]. This present findings reveals that the active sites of [C_4MIM][OMs] molecules could attached on the mild steel surface. The LUMO distribution portray receptor orbital of the inhibitor molecules [77,78]. The energy gap is defined as the difference of highest occupied molecular orbital and the lowest unoccupied molecular orbital ($\Delta E = E_{LUMO} - E_{HOMO}$). The difference in energy value indicates high inhibition efficiency of [C_4MIM][OMs] molecules. As reported by Koopmans's model, it describes the relationship linking HOMO and LUMO regions as given in Eq. 13 and 14.

$$I = -E_{HOMO} \tag{13}$$

$$A = -E_{LUMO} \tag{14}$$

The efficiency of [C_4MIM][OMs] molecules was studied ascertaining the variables and estimating the global parameters like softness (σ_s), electronegativity index (X_e), chemical hardness (η_d), electrophilicity (w_e), fraction of electron transported (ΔN), dipole moment (μ) as well as the back donation (ΔE_T) during interaction using Eqs. (15)–(21) [77,79].

$$\eta_d = \frac{IE - EA}{2} \tag{15}$$

$$\sigma_S = \frac{1}{\eta_d} \tag{16}$$

$$X_e = \frac{IE + EA}{2} \tag{17}$$

$$w_e = \frac{(IE + EA)^2}{8(IE + EA)} \tag{18}$$

$$\Delta N = \frac{X_{es} - X_i}{2(\eta_m + \eta_i)} \tag{19}$$

$$\mu = \sqrt{w_e 2\eta_d} \tag{20}$$

$$\Delta E_T = -\frac{\eta}{4} \tag{21}$$

The computed values are shown in Table 8, it shows that global hardness is 1.5278 and greater than zero advocating charge transport from [C_4MIM][OMs] molecules to the steel surface. Also, total change in energy during back donation (ΔE_T) was less than zero (−0.3820), evidently implies back donation from the mild steel surface to the [C_4MIM][OMs] molecule thereby relating total change in energy to the global hardness of the particle according to Eq. (21) [79]. The electronegativity (X_e) provides an idea for [C_4MIM][OMs] reactivity and selectivity as corrosion inhibitor [77]. According to Refs. [80,81] electrophilicity index (w_e) describes the capacity of [C_4MIM][OMs] molecules to accept or donate electron, calculated value of w_e (0.8899) suggests electron donation to the metal, which indicates greater reactivity of [C_4MIM][OMs] molecules and exhibited high inhibition level. The fraction of electron transferred (ΔN) arises as a result of flow of electron from a less electronegativity molecules to the electronegativity metal [73].

Table 8
Estimated chemical quantum parameters for [C_4MIM][OMs] particle.

DFT parameters	[C_4MIM][OMs]
E_{HOMO} (eV)	−4.0640
E_{LUMO} (eV)	−1.0085
ΔE (eV)	3.0555
Ionization potential; *IE* (eV)	4.0640
Electron affinity; *EA* (eV)	3.0555
Hardness; η_d (eV)	1.5278
Softness; σ_s (eV^{-1})	0.6545
Fraction of electron transferred; ΔN (e)	2.2909
Electrophilicity index; w_e (eV)	0.8899
Electronegativity parameter X_e (eV)	3.5598
Back donation ΔE_T	−0.3820
Dipole moment μ (debyes)	1.6490

According to Ref. [40], when small amount of electron transported is greater than zero, there is movement of electron from the inhibitor molecule to the metal surface. Appreciably, the amount of electron donated is related to the high inhibition efficiency. This implies that the inhibition ability of inhibitor [C_4MIM][OMs] molecule is enhanced when $\Delta N < 3.6$ [14]. Dipole moment (μ) is employed to predict the ability of a corrosion inhibitor to inhibit corrosion. Dipole moment estimates the polarity in bond and quantifies the volume of [C_4MIM][OMs] molecules. An increase in value of μ, makes the inhibitor molecules easier to adsorb and bond onto the mild steel surface [72]. Also, literature reveals that corrosion inhibition efficiency do not depend on the value of μ [82]. Interestingly, the result exhibited in Table 8 shows that [C_4MIM][OMs] molecules have a considerable dipole moment value which facilitates adsorption onto the mild steel surface.

As evidenced, Fig. 8 exhibit the surface probing of [C_4MIM][OMs] molecules together with Fe (110). This result was performed *via* the MD-simulation approach to envisage inhibition characteristics of [C_4MIM][OMs] molecules on the Fe (110) plane in gas and liquid phase. Fig. 8a–b shows the top view and the side views of [C_4MIM][OMs] molecules in gas phase. Also, Fig. 8(c–e) exhibits the top view, side and front view for [C_4MIM][OMs] molecules on the Fe (110) plane in liquid phase. Based on the simulation, a flat adsorption of [C_4MIM][OMs] molecule was seen on the Fe surface in a well arrange form. In all, the adsorption position of the inhibitor is directly in contact with the mild steel surface hence, promoting degree of surface coverage. This action exhibited by [C_4MIM][OMs] molecules

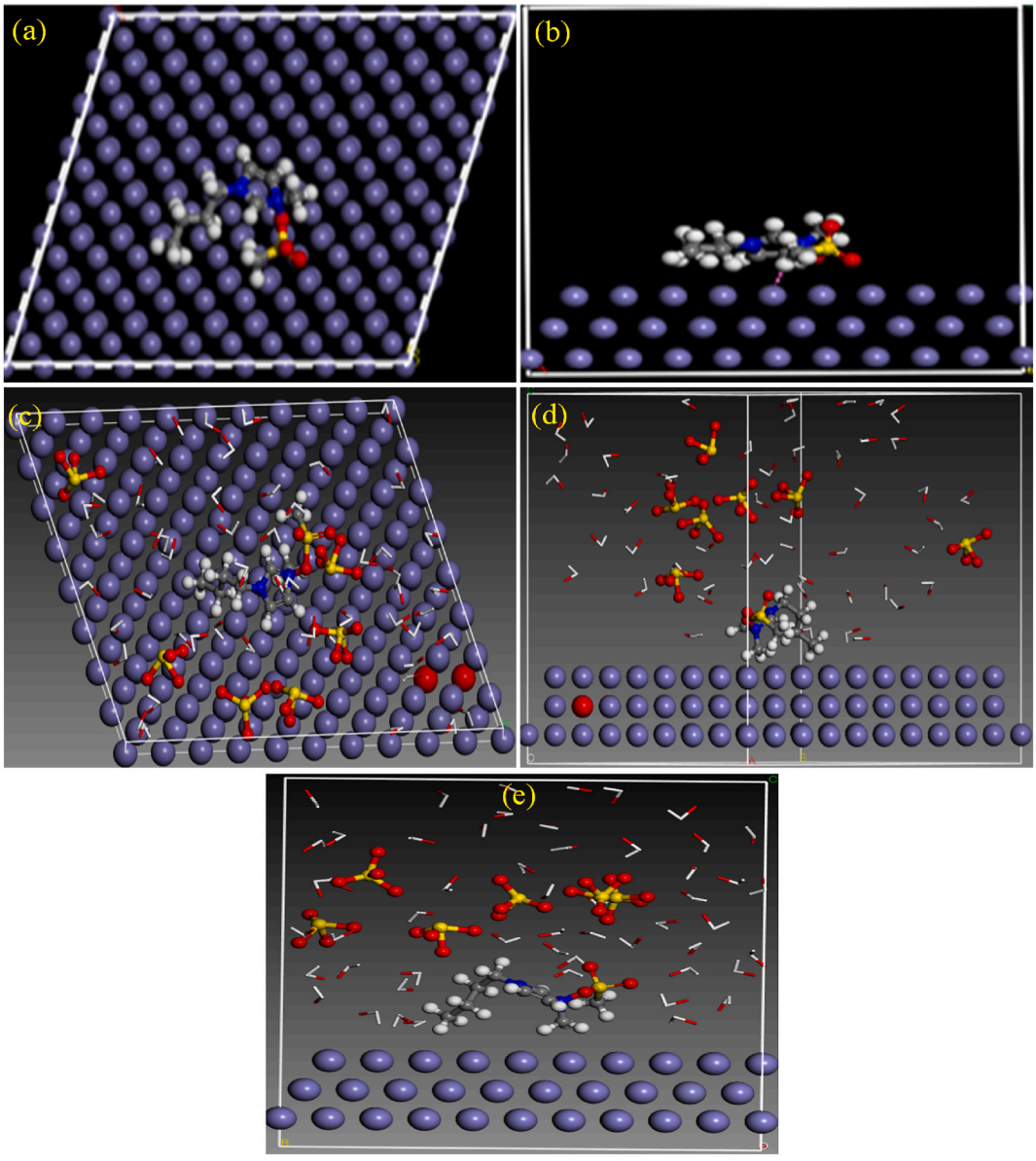

Fig. 8. (a) the on-top view; (b) the edge sight of smallest energy adsorption model for Fe (110) plane inside gas phase; (c); (d) and (e) top, edge and front sight for Fe (110) facet in liquid phase. Atom legend: white = H; gray = C; red = O; blue = N and yellow = S.

could be accredited to the heteroatoms present in the inhibitor.

3.7. Mathematical and statistical analysis

In order to evaluate and predict the experimental data, 3D-surface plots were employed to examine the parameters that possess notable outcomes in the corrosion inhibition process. As evidenced, Fig. 9 shows the physical interaction of [C_4MIM][OMs] molecules on the mild steel with the input variables. The effect of temperature, time and [C_4MIM][OMs] concentration were considered. A graph of the response *versus* experimental was plotted (Fig. 9a), a linear relationship was observed showing a good model. Fig. 9b–c, revealed that increase in [C_4MIM][OMs] concentration at 0.8 g L^{-1} enhances the surface coverage of the mild steel. The effect of temperature on the output was studied as shown in Fig. 9b and d). Increasing the temperature up to 323 K weakened the [C_4MIM][OMs] thus, dispersing the inhibitor molecules from the mild steel surface. As temperature increases, the magnitude of corrosion increases owing to the dispersion of [C_4MIM][OMs] molecules on the metal surface leaving the mild steel prone to acid penetration. Effect of exposure time was considered (Fig. 9c and d). This normally examines the strength of the barrier film layer formed on the steel surface. In the first instance, adsorption of [C_4MIM][OMs] molecules on mild steel was observed, but at some points, further rise in temperature decreases the surface coverage and promotes corrosion. This mechanism reveals a negative factor affecting the degree of metal protection over time.

Conversely, at optimum concentration of 0.8 g L^{-1} [C_4MIM][OMs] remarkable inhibition level was attained due to the presence of more [C_4MIM][OMs] molecules required for adsorption on the mild steel surface. As evidenced, Table 9 shows that gradual rise in [C_4MIM][OMs] concentration, increases the metal surface coverage owing to its molecular structure and composition. The inhibition efficiency of 85.71% was recorded in Table 9. Similarly, at the expiration of 3hr of immersion, the inhibitor molecules seem to reach equilibrium state, therefore no observable change was noted afterwards. Furthermore, Table 10 shows that estimated inhibition efficiency was 84.06% at of 0.76 g L^{-1} [C_4MIM][OMs] concentration, 313 K temperature and 2.78hr of immersion time. A percentage deviation of 1.96% and a standard deviation of 1.17% of the inhibition efficiency were achieved. The small estimate of the standard deviation signifies that the computed value of the inhibition efficiency at optimum conditions are close to the mean value and correlates with the experimental result.

Where Factor 1 = A: inhibitor conc. (g/L); Factor 2 = B: temperature (K); Factor 3 = C: time (hr); Response Z = IE: inhibition efficiency.

3.7.1. Model suitability

Three variables were extensively connected with a response employing quadratic design equation. The regression model from the experimental data recorded as coded factor is presented as Eq. (22).

$$Z = +86.03 + 2.95A - 3.41B + 5.93C + 1.31AB - 1.56AC - 7.06A^2 - 10.77B^2 - 15.27C2 \quad (22)$$

Owing to the input parameters examined, the influence of one parameter is acceptably complacent by the measure of one element. In this regard, favorable action stipulates joined effect, on the other hand an unfavorable action designates opposed operation.

Furthermore, to adequately scrutinize the proposed model suitability, analysis of variance (ANOVA) were employed [83]. The ANOVA calculations were shown in Table 11. The F-distribution value of 147.07 was recorded showing high F-value and depicts that the design is statistically significant. This might occur due to noise, attributed to the heteroatoms of the inhibitor molecules. The coefficient of determination (R^2) of the design is 0.9943 and it revealed a satisfactory fitting connecting estimated value and empirical data. Furthermore, R^2 value shows high-level reliance and link connecting the estimated inhibition value [84]. Predicted R^2 value is 0.9415. This is justifiable with Adjusted R^2 value of 0.9858, Adeq precision evaluates the linear line to the scattered point. A proportion bigger than 4 is recommended. The proportion value of 37.3464 shows the accuracy of the design. From Table 11, p-value is less than 0.0500. Thus, coded factors of A, B, C, AC, A^2, B^2, C^2 are the outstanding parameters for the inhibition process.

4. Conclusion

- [C_4MIM][OMs] based ionic liquid acts as a good corrosion inhibitor for mild steel in acidic environment.
- The adsorption isotherm obeys Langmuir adsorption model.
- The electrochemical data indicates that [C_4MIM][OMs] based ionic liquid acted as a mixed type inhibitor with cathodic predominance.
- The theoretical studies (DFT/MD-simulation) validates the experimental findings.
- The statistical design generated *via* RSM analyzed the quadratic interactions between the input parameters and predicted response.

Author contribution statement

Daniel Iheanacho Udunwa: Performed the experiments; Wrote the paper.
Okechukwu Dominic Onukwuli, Mathew Chukwudi Menkiti: Conceived and designed the experiments.
Valentine Chikaodili Anadebe: Analyzed and interpreted the data.
Maduabuchi Arinzechukwu Chidiebere: Contributed reagents, materials, analysis tools or data.

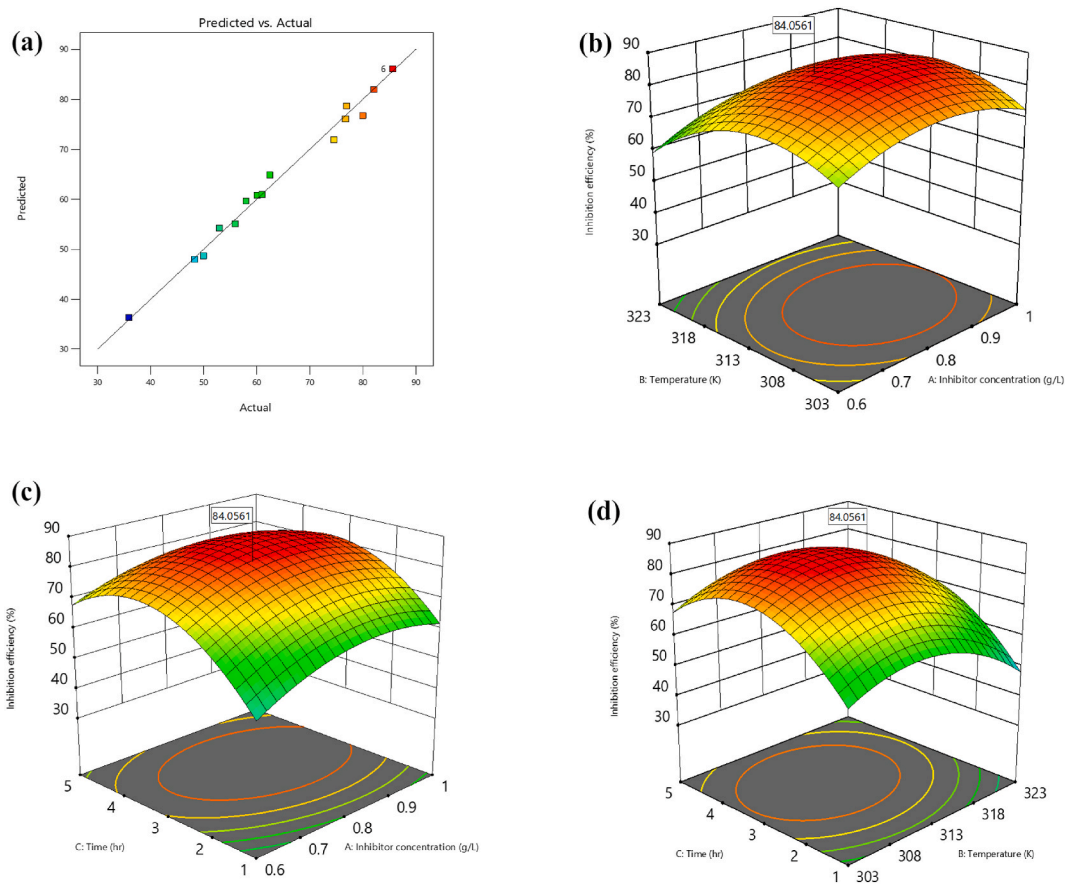

Fig. 9. RSM plot for low-carbon steel in 1 M H_2S0_4: (a) Response against experimental IE%; (b) temperature against inhibitor concentration; (c) time against inhibitor concentration; and (d) time against temperature.

Table 9
RSM prediction for low-carbon steel in 1 M H_2SO_4.

Std	Run	Factor 1	Factor 2	Factor 3	Response 1
13	1	0.8	313	1	62.50
6	2	1.0	303	5	61.00
15	3	0.8	313	3	85.71
7	4	0.6	323	5	53.00
9	5	0.6	313	3	76.79
20	6	0.8	313	3	85.71
3	7	0.6	323	1	36.00
17	8	0.8	313	3	85.71
5	9	0.6	303	5	60.15
18	10	0.8	313	3	85.71
12	11	0.8	323	3	74.58
11	12	0.8	303	3	76.92
8	13	1.0	323	5	58.00
16	14	0.8	313	3	85.71
10	15	1.0	313	3	82.14
1	16	0.6	303	1	50.00
19	17	0.8	313	3	85.71
14	18	0.8	313	5	80.00
4	19	1.0	323	1	48.34
2	20	1.0	303	1	56.00

Table 10
Validation calculations for mild steel in 1 M H_2SO_4.

Position	[C_4MIM][OMs] (gL^{-1})	Time (hr)	Temperature (K)	Estimated (IE %)	Experimental (IE %)	Percentage Deviation (%)	Standard Deviation (%)
Optimal result	0.76 g L^{-1}	2.78	313.97	84.06	85.71	1.96	1.17
Duplicate result	0.8 g L^{-1}	3.00	313.00	84.06	85.69	1.93	1.15

Table 11
ANOVA result for response surface methodology for low-carbon steel in 1 M H_2SO_4.

Source	Sum of Squares	Df	Mean Square	F-value	p-value Prob > F
Model	4690.84	9	521.20	147.07	<0.0001 Significant
A-Inhibitor concentration	87.26	1	87.26	24.62	0.0006
B-Temperature	116.62	1	116.62	32.91	0.0002
C-Time	351.77	1	351.77	99.26	<0.0001
AB	13.76	1	13.76	3.88	0.0771
AC	19.50	1	19.50	5.50	0.0409
BC	16.56	1	16.56	4.67	0.0559
A^2	136.96	1	136.96	38.65	<0.0001
B^2	319.12	1	319.12	90.05	<0.0001
C^2	641.42	1	641.42	180.99	<0.0001
Residual	35.44	10	3.54		
Lack of Fit	35.44	5	7.09		
Pure Error	0.0000	5	0.0000		
Cor Total	4726.27	19			
Adj R- square	0.9858				
Pre-R – square	0.9415				

Data availability statement

Data will be made available on request.

Declaration of interest's statement

The authors declare no conflict of interest.

Declaration of competing interest

The authors declare that they have no known competing financial interests or personal relationships that could have appeared to influence the work reported in this paper.

Acknowledgements

Department of Polymer and Textile Engineering (PTE), FUTO, Imo State, Nigeria and Nnamdi Azikiwe University (UNIZIK), Awka, Anambra State, Nigeria are appreciatively acknowledged by Udunwa for the provision of necessary laboratory equipment for this research work. D. I. Udunwa also acknowledged the African Centre of Excellence in Future Energies and Electrochemical System, Federal University of Technology, Owerri, Imo State, Nigeria, for their contributions. Council of Scientific and Industrial Research (CSIR), India, and The World Academy of Sciences (TWAS), Italy are gratefully acknowledged by Anadebe for the CSIR-TWAS Postgraduate Fellowship (Award No. 22/FF/CSIR-TWAS/2019) to pursue his Ph.D. research program in CSIR-CECRI, India. V.C. Anadebe, acknowledges Alex Ekwueme Federal University Ndufu-Alike, Ebonyi State, Nigeria, for a research leave to study his Ph.D. in CSIR-CECRI, India.

References

[1] A.A. Khadom, M.M. Kadhim, R.A. Anaee, H.B. Mahood, M.S. Mahdi, A.W. Salman, Theoretical evaluation of Citrus Aurantium leaf extract as green inhibitor for chemical and biological corrosion of mild steel in acidic solution: statistical, molecular dynamics, docking, and quantum mechanics study, J. Mol. Liq. 343 (2021), 116978.
[2] A.A. Khadom, S.A. Jassim, M.M. Kadhim, N.B. Ali, Influence of apricot constituents as eco-friendly corrosion inhibitor for mild steel in acidic medium: a theoretical approach, J. Mol. Liq. 347 (2022), 117984.
[3] K.H. Rashid, A.A. Khadom, 3-Methoxypropyl-amine as corrosion inhibitor for X80 steel in simulated saline water, J. Mol. Liq. 319 (2020), 114326.
[4] Y. Li, S. Zhang, Q. Ding, B. Qin, L. Hu, Versatile 4,6-dimethyl-2- mercaptopyrimidine based ionic liquids as high-performance corrosion inhibitors and lubricants, J. Mol. Liq. 284 (2019) 577–585.

[5] M.H. Shahini, M. Keramatinia, M. Ramezanzadeh, B. Ramezanzadeh, G. Bahlakeh, Combined atomic-scale/DFT-theoretical simulations & electrochemical assessments of the chamomile flower extract as a green corrosion inhibitor for mild steel in HCl solution, J. Mol. Liq. 342 (2021), 117570.

[6] S.M. Lashgari, G. Bahlakeh, B. Ramezanzadeh, Detailed theoretical DFT computation/molecular simulation and electrochemical explorations of Thymus vulgaris leave extract for effective mild-steel corrosion retardation in HCl solution, J. Mol. Liq. 335 (2021), 115897.

[7] M.H. Shahini, M. Ramezanzadeh, G. Bahlakeh, B. Ramezanzadeh, Superior inhibition action of the Mish Gush (MG) leaves extract toward mild steel corrosion in HCl solution: theoretical and electrochemical studies, J. Mol. Liq. 332 (2021), 115876.

[8] A. Salmasifar, M. Edraki, E. Alibakhshi, B. Ramezanzadeh, G. Bahlakeh, Theoretical design coupled with experimental study of the effectiveness of the inhibitive molecules based on Cynara scolymus L extract toward chloride-induced corrosion of steel, J. Mol. Liq. 332 (2021), 115742.

[9] I.B. Obot, I.B. Onyeachu, S.A. Umoren, M.A. Quraishi, A.A. Sorour, T. Chen, N. Aljeaban, Q. Wang, High temperature sweet corrosion and inhibition in the oil and gas industry: progress, challenges and future perspectives, J. Pet. Sci. Eng. 185 (2020), 106469.

[10] A. Zouitini, Y.K. Rodi, Y. Ouzidan, F.O. Chahdi, I. Abdel-Rahman, E.M. Essassi, A. Aouniti, B. Hammouti, H. Elsmsellem, Corrosion inhibition studies of new synthesized 1,4-diocytl-6-methyl-1,4-dihydroquinoxaline-2,3-dione on mild steel in 1.0M HCl solution using gravimetric and electrochemical techniques supported by theoretical DFT calculation, Int. J. Corros. Scale Inhibit. 8 (2) (2019) 225–240.

[11] T.A. Salman, O.A. Jawad, M.A.M. Hussien, A.A. Amiery, L. Mohamed, A.A.H. Kadium, M.S. Takriff, Novel ecofriendly corrosion inhibitor of mild steel in strong acid environment: adsorption studies and thermal effects, Int. J. Corros. Scale inhibit 8 (4) (2019) 1123–1137.

[12] X. Luo, C. Ci, J. Li, K. Lin, S. Du, H. Zhang, X. Li, Y.F. Cheng, J. Zhang, Y. Liu, 4-aminoazobenzene modified natural glucomannan as a green eco-friendly inhibitor for mild steel in 0.5 M HCl solution, Corrosion Sci. 151 (2019) 132–142.

[13] M.M. Solomon, A.U. Saviour, M.A. Quraishi, S. Mohammad, Myristic acid based imida-zoline derivative as effective corrosion inhibitor for steel in 15 % HCl medium, J. Colloid Interface Sci. 551 (2019) 47–60.

[14] Y. Qiang, S. Zhang, L. Guo, X. Zheng, B. Xiang, S. Chem, Experimental and theoretical studies of four allyl imidazolium-based ionic liquids as green inhibition for copper in sulfuric acid, Corrosion Sci. 119 (2017) 68–78.

[15] K.K. Anupama, K. Ramya, K.M. Shaimy, A. Joseph, Adsorption and electrochemical studies of pimenta dioica leaf extracts as corrosion inhibitor for mild steel in hydrochloric acid, Mater. Chem. Phys. 167 (2015) 28–41.

[16] A. Saxena, D. Prasad, R. Haldhar, G. Singh, A. Kumar, Use of Sida cordifolia extracts as green corrosion inhibitor for mild steel in 0.5 M H2SO4, J. Environ. Chem. Eng. 6 (1) (2018) 694–700.

[17] A.A. Khadom, A.F. Hassan, B.M. Abod, Evaluation of environmentally friendly inhibitor for galvanic corrosion of steel-copper couple in petroleum waste water, Process Saf. Environ. Protect. 98 (2015) 93–101.

[18] M.N. El-Hadda, A.S. Fouda, A.F. Hassan, Data from chemical, electrochemical and quantum chemical studies for interaction between Cephapirin drug as an eco-friendly corrosion inhibitor and carbon steel surface in acidic medium, Chem. Data Collection 22 (2019) 100251.

[19] S. Padhan, T.K. Rout, U.G. Nair, N-doped and Cu, N-doped carbon dots as corrosion inhibitor for mild steel corrosion in acid medium, Colloids Surf., A: Physiochem. Eng. Asp. 653 (2022), 129905.

[20] A. Singh, N. Soni, Y. Deyuan, A. Kumar, A Combined electrochemical and theoretical analysis of environmentally benign polymer for corrosion protection of N80 steel in sweet corrosive environment, Results Phys. 13 (2019), 102116.

[21] P. Deepa, R. Padmalatha, Corrosion behavior of 6063 aluminum alloy in acidic and alkaline media, Arab. J. Chem. 10 (2017) S2234–S2244.

[22] D.I. Udunwa, O.D. Onukwuli, M. Omotioma, Corrosion control of aluminium alloy in HCl using extract of Ocimum gratissimum as inhibitor, Der Pharma Chem. 9 (19) (2017) 48–59.

[23] V.C. Anadebe, V.I. Chukwuike, S. Ramanathan, R.C. Barik, Cerium-based metal organic framework (Ce-MOF) as corrosion inhibitor for API 5L X65 steel in CO_2-saturated brine solution: XPS, DFT/MD-simulation, and machine learning model prediction, Process Saf. Environ. Protect. 168 (2022) 499–512.

[24] M. Mobin, R. Aslam, Experimental and theoretical study on corrosion inhibition performance of environmentally benign non-ionic surfactants for mild steel in 3.5 % NaCl solution, Process Saf. Environ. Protect. 114 (2018) 279–295.

[25] M. Galai, M. Rbaa, H. Serrar, M. Quakki, A. Ech-Chebab, A.S. Abousalem, E. Ech-Chihbi, K. Dahmani, S. Boukhris, A. Zarrouk, M. EbnTouhami, S-Thiazine as effective inhibitor of mild steel corrosion in HCl solution: synthesis, experimental, theoretical and surface assessment, Colloids Surf., A: Physiscochem. Eng. Asp. 613 (2021), 126127.

[26] D.S. Zinad, Q.A. Jawad, M.A.M. Hussien, A. Mahal, L. Mohammed, A.A. Amiery, Adsorption, temperature and corrosion inhibitor for mild steel in acid medium: gravimetric and theoretical investigations, Int. J. Corros. Scale Inhibit. 9 (1) (2020) 134–151.

[27] L. Guo, M. Zhu, J. Chang, R. Thomas, R. Zhang, P. Wang, X. Zheng, Y. Lin, R. Marzouki, Corrosion inhibition of N80 steel by newly synthesized imidazoline based ionic liquid in 15% HCl medium: experimental and theoretical investigations, Int. J. Electrochem. Sci. 16 (2021), 211139.

[28] S. Ozturk, H. Gerengi, M.M. Solomon, G. Gece, A. Yildirim, M. Yildiz, A newly synthesized ionic liquid as an effective corrosion inhibitor for carbon steel in HCl medium: a combined experimental and computational studies, Mater. Today Commun. 29 (2021), 102905.

[29] E. Berdimurodov, A. Kholikov, K. Akbarov, L. Guo, S. Kaya, K.P. Katin, D.K. Verma, M. Rbaa, O. Dagdag, R. Haldhar, Novel bromide–cucurbit [7] uril supramolecular ionic liquid as a green corrosion inhibitor for the oil and gas industry, J. Electroanal. Chem. 901 (2021), 115794.

[30] A.L. Chong, J.I. Mardel, D.R. MacFarlane, M. Forsyth, A.E. Somers, Synergistic corrosion inhibition of mild steel in aqueous chloride solutions by an imidazolinium carboxylate salt, ACS Sustainable Chem. Eng. 4 (3) (2016) 1746–1755.

[31] M.M. Barakat, M.A. Deyab, M.I. Nessim, S.S. Abd El-Rehim, Q. Mohsen, The controlling role of new imidazole-based ionic liquids on the corrosion rate of steel rebars in the cement pore solution, J. Mol. Liq. 329 (2021), 115442.

[32] Q. Zhang, L. Guo, Y. Huang, R. Zhang, A.G. Ritacca, S. Leng, X. Zheng, Y. Yang, A. Singh, Influence of an imidazole-based ionic liquid as electrolyte additive on the performance of alkaline Al-air battery, J. Power Sources 564 (2023), 232901.

[33] L.H. Madkour, I.H. Elshamy, Experimental and computational studies on the inhibition performance of benzimidazole and its derivatives for corrosion of copper in nitric acid, Int. J. Ind. Chem. 7 (2016) 195–221.

[34] Y. Sasikumar, A.S. Adekunle, L.O. Olasunkanmi, A. Adekunle, I. Bahadur, Experimental, quantum and Monte-Carlos simulation studies on corrosion inhibition of some alkyl immidazolium ionic liquids containing tetraflouroborate anion on mild steel in acid medium, J. Mol. Liq. 211 (2015) 105–118.

[35] M.M. Shaban, N.A. Negm, R.K. Farag, A.A. Fadda, A.E. Gomma, A.A. Farag, M.A. Migahed, Anti-corrosion, antiscalant and anti-microbal performance of some synthesized trimeric cationic imidazolium salts in oilfield applications, J. Mol. Liq. 351 (2022), 118610.

[36] W. Xiaohong, A. Ailing, L. Dongquan, T. Mohd, L. Hao, L. Yuanhua, Imidazolium-based ionic liquids as efficient corrosion inhibitor for AA6061 alloy in HCl solution, Materials 13 (2020) 4672.

[37] J. Wang, A. Singh, M. Talha, X.I. Luo, X. Deng, Y. Lin, Electrochemical and theoretical study of Imidazole derivative as effective corrosion inhibitor for aluminum, RSC Adv. 5 (16) (2015) 11697–11713.

[38] M.H. Sliem, A.B. Radwan, F.S. Mohamed, N.A. Alnuaimi, A.M. Abdullahi, An efficient green ionic liquid for the corrosion inhibition of reinforcement steel in neutral and alkaline highly saline simulated concrete pore solutions, Sci. Rep. 10 (2020), 14565.

[39] S.K. Shetty, A.N. Shetty, Ionic liquid as an effective corrosion inhibitor on 6061 Al-15 Vol.Pct. SiC (p) composite in 0.1M H_2SO_4 medium-an ecofriendly approach, Can. Chem. Trans. 3 (2015) 41–64.

[40] G. Parveen, S. Bashir, A. Thakur, S.K. Saha, P. Banerjee, A. Kumar, Experimental and computational studies of imidazolium based ionic liquid 1-methyl-3-propylimidazolium iodide on mild steel corrosion in acidic solution, Mater. Res. Express 7 (1) (2019), 016510.

[41] V.C. Anadebe, O.D. Onukwuli, M. Omotioma, N.A. Okafor, Experimental, theoretical modeling and optimization of inhibition efficiency of pigeon pea leaf extract as anti-corrosion agent of mild steel in acid environment, Mater. Chem. Phys. 233 (2019) 120–132.

[42] V.C. Anadebe, P.C. Nnaji, O.D. Onukwuli, N.A. Okafor, F.E. Abeng, V.I. Chukwuike, C.C. Okoye, I.I. Udoh, M.A. Chidiebere, L. Guo, R.C. Barik, Multidimensional insight into the corrosion inhibition of salbutamol drug molecule on mild steel in oilfield acidizing fluid: experimental and computer aided modeling approach, J. Mol. Liq. 349 (2022), 118482.

[43] A.S. Khan, Z. Man, A. Arvina, M.A. Bus, A. Nasrullah, Z. Ullah, A. Sarwono, N. Mohammad, Dicationic imidazolium based ionic liquids synthesis and properties, J. Mol. Liq. 227 (2016) 98–105.

[44] V.C. Anadebe, V.I. Chukwuike, M.A. Chidiebere, R.C. Barik, Synthesis, Characterization, and evaluation of Co-MOF based ZIF-67 for CO_2 corrosion inhibition of X65 steel: insights from electrochemical studies and a machine learning algorithm, J. Phys. Chem. C 127 (20) (2023) 9871–9886.

[45] C. Verma, L.O. Olasunkanmi, I. Bahadur, H. Lgaz, M.A. Quraishi, J. Haqure, M. Sherif, E.E. Ebenso, Experimental, density functional theory and molecular dynamics support adsorption behavior of environmental benign imidazolium based ionic liquids on mild steel surface in acidic medium, J. Mol. Liq. 273 (2019) 1–5.

[46] P. M Ejikeme, S.G. Umana, M.C. Menkiti, O.D. Onukwuli, Inhibition of mild steel and aluminum corrosion in 1M H_2SO_4 by leaves extract of African breadfruit, Int. J. Mater. Chem. 5 (1) (2015) 14–23.

[47] I. Wei, Z. Chen, X. Guo, Inhibition behavior of an imidazoline inhibitor for carbon steel in a supercritical CO_2/H_2O system, J. Electrochem. Soc. 164 (2017) C602–C609.

[48] C.O. Alkalezi, M.C. Okafor, E.E. Oguzie, Experimental and DFT evaluation of adsorption and inhibitive properties of Moringa oliefera extract on mild steel corrosion in acidic media, Arab. J. Chem. 13 (12) (2020) 9270–9282.

[49] F.M. Sani, B. Brown, S. Nesic, An electrochemical study of the effect of high salt concentration on uniform corrosion of carbon steel in aqueous CO_2 solutions, J. Electrochem. Soc. 168 (5) (2021), 051501.

[50] V.C. Anadebe, O.D. Onukwuli, M. Omotioma, N.A. Okafor, Optimization and electrochemical study on the control of mild steel corrosion in hydrochloric acid solution with bitter kola leaf extract as inhibitor, S. Afr. J. Chem. 71 (2018) 51–61.

[51] M.A. Hegazi, A.A. Nazeer, K. Shalabi, Electrochemical studies on the inhibition behavior of copper corrosion in pickling acid using quaternary ammonium salts, J. Mol. Liq. 209 (2015) 419, 27.

[52] P.R. Prabhu, P. Deepa, R. Padmalatha, Analysis of Garcinia indica Choisy extract as friendly corrosion inhibitor for aluminum in phosphoric acid using the design of experiment, J. Mater. Res. Technol. 9 (3) (2020) 3622, 31.

[53] N.S. Abdelshafi, A.S. Halim, Corrosion inhibition of aluminum in 1 M HCl by novel pyrimidine derivatives, EFM measurements, DFT calculations and MD simulation, Arab. J. Chem. 15 (1) (2022), 103456.

[54] T.A. Salman, A.A. Almiery, L.M. Shaker, A.A.H. Khadhum, M.S. Takriff, A Study of the inhibition of mild steel corrosion in hydrochloric acid environment by 4-methyl-2- (pyrdin-3-yl) thiazole-5- carbohydrate, Int. J. Corros. Scale Inhibit. 8 (4) (2019) 1035–1059.

[55] V.C. Anadebe, O.D. Onukwuli, F.E. Abeng, N.A. Okafor, J.O. Ezeugo, C.C. Okoye, Electrochemical kinetics, MD-simulation and multi-input single-output (MISO) modeling using adaptive neuro-fuzzy inference system (ANFIS) prediction for dexamethasone drug as eco-friendly corrosion inhibitor for mild steel in 2M HCl electrolyte, J. Taiwan Inst. Chem. Eng. 115 (2020) 251–265.

[56] L. Messaadia, O.I.D. El-Mouden, A. Anejjar, M. Messali, R. Salghi, O. Bernali, O. Cherkaoui, A. Lallam, Adsorption and corrosion inhibition of new synthesized pyridazinium-based ionic liquid on carbon steel in 0.5M H_2SO_4, J. Mater. Environ. Sci. 6 (2015) 598–606.

[57] E. Alibakhshi, M. Ramezanzadeh, S.A. Haddadi, G. Bahlakeh, B. Ramezanzadeh, M. Mahdavian, Persian liquorice extract as highly efficient sustainable corrosion inhibitor for mild steel in sodium chloride solution, J. Clean. Prod. 210 (2019) 660–672.

[58] A. Farhadian, M.A. Varfolomeev, M. Razaeisadat, A.P. Semenov, A.S. Stoporev, Towards a bio-based hybrid inhibition of gas hydrate and corrosion for flow assurance, Energy 210 (2020), 118549.

[59] A. Singh, K.K. Ansari, K.R. Quraishi, P. Banerjee, Corrosion inhibition and adsorption of imidazolium based ionic liquid over P110 steel surface in 15% HCl under static and dynamic condition: experimental, surface and theoretical analysis, J. Mol. Liq. 323 (2020), 114606.

[60] M.E. Ikpi, F.E. Abeng, Electrochemical impedance spectroscopy and gravimetric study of the corrosion inhibition of API 5L X-52 steel in HCl medium by levofloxacin, Int. J. Sci. Res. 6 (2017) 623–628.

[61] M. Filali, E.M. El-Hadrani, A. Ben-Tama, B. Hafez, I. Abdel-Rahaman, A. Harrach, H. Elmsellem, B. Hammouti, M. Mokhtani, S.E. Stiriba, M. Julve, 3,6-D (pyradin-2-yl) pyradizine derivatives as original and new corrosion inhibitors in support of mild steel: experimental studies and DFT investigation, Int. J. Corros. Scale Inhibit. 11 (1) (2019) 93–109.

[62] S.A. Umoren, Polypropylene glycol: a novel corrosion inhibitor for X 60 pipeline steel in 15% HCl solution, J. Mol. Liq. 219 (2016) 946–958.

[63] Z. Xuanxuan, T. Bochuan, Corrosion inhibition performance of three antibacterial agents for mild steel in 1M HCl solution at different temperatures: experimental and theoretical studies, Int. J. Electrochem. Sci. 13 (2018) 11388–11404.

[64] B. Tan, S. Zhang, Y. Qiang, I. Guo, I. Feng, C. Liao, Y. Xu, S.A. Chen, A combined experimental and theoretical study of the inhibition effect of three disulfide-based flavouring agent for copper corrosion in 0.5M sulfuric acid, J. Colloid Interface Sci. 526 (2018) 268–280.

[65] C. Verma, M.A. Quraishi, E. E Ebenso, B. Indra, A green and sustainable approach for mild steel acidic corrosion inhibition using leaves extract: experimental and DFT studies, J. Bio. Tribo. Corros. 4 (3) (2018) 1–12.

[66] X. Klodian, F. Matgaz, Organic corrosion inhibitors for aluminium and its alloys in chloride and alkaline solutions: a review, Arab. J. Chem. 12 (2019) 4646–4663.

[67] P. Nayak, P.P. Kumari, S.A. Rao, Electrochemical approach to interfacial adsorption and inhibitory performance of (2E) -2- [(H - imidazole2yl) methylidene] Hydrazine1-carbothioamide for corrosion mitigation, Chem. Data Collect. 38 (2022), 100826.

[68] B.J. Usman, Z.M. Gasem, S.A. Umoren, M.M. Solomon, Eco-friendly 2-thiobarbituric acid as a corrosion inhibitor for API 5L X60 steel stimulated sweet oilfield environment: electrochemical and surface analysis studies, Sci. Rep. 9 (2019) 1–17.

[69] V.C. Anadebe, V.I. Chukwuike, V. Selvaraj, A. Pandikumar, R.C. Barik, Sulfur-doped graphitic carbon nitride (Sg-C_3N_4) as an efficient corrosion inhibitor for X65 pipeline steel in CO_2-saturated 3.5 % NaCl solution: electrochemical, XPS and Nanoindentation Studies, Process Saf. Environ. Protect. 164 (2022) 715–728.

[70] V.C. Anadebe, C.S. Okafor, O.D. Onukwuli, Electrochemical, molecular dynamics, adsorption studies and anti-corrosion activities of Moringa leaf biomolecules on carbon steel surface in alkaline and acid environment, Chemical Data Collections 28 (2020), 100437.

[71] H. Challouf, N. Souissi, M.B. Messaouda, R. Abidi, A. Madani, Origanum majorana extracts as mild steel corrosion green inhibitor in aqueous chloride medium, J. Environ. Protect. 7 (4) (2016) 532–544.

[72] B. Hassan, O. Rachid, B. El Ibrahimi, A.O. Hichan, A. Younness, B. Bouchra, S. El Issami, H. Mustapha, B. Lahcen, L. Christophe, Furfural analogs as sustainable corrosion inhibitors- predictive efficiency using DFT and Monte Carlos simulations on the Cu (111), Fe (110), Al (111) and Sn (111) surfaces in acid media, Sustainability 12 (2020) 3304.

[73] M. El Faydy, F. Benhiba, B. Lakhrissi, M.E. Touhami, I. Warad, F. Bentiss, A. Zarrouk, The inhibitive impact of both kinds of 5-isothiocyanatomethyl-8-hydroxyquinoline derivatives on the corrosion of carbon steel in acidic electrolyte, J. Mol. Liq. 295 (2019), 111629.

[74] H.M. Abd El-Lateef, K. Shalabi, A.A. Abdelhamid, One-pot synthesis of novel triphenyl hexyl imidazole derivatives catalyzed by ionic liquid for acid corrosion inhibition of C1018 steel: experimental and computational perspectives, J. Mol. Liq. (2021), 116081.

[75] A. Thoume, A. Elmakssoudi, D.B. Left, R. Achagar, I.N. Irahal, M. Dakir, M. Azzi, M. Zertoubi, Dibenzylidenecyclohexanone as new corrosion inhibitor of carbon steel in 1M HCl, J. Bio Tribo Corros. 7 (2021) 130.

[76] C.M. Fernandes, V.G.S. Pina, L.X. Alvarez, A.C.F. de Albuquerque, F.M. dos Santos Junior, A.M. Barriors, J.A.C. Valasco, E.A. Ponzio, Use of a theoretical prediction method and quantum chemical calculations for the design, synthesis and experimental evaluation of three green corrosion inhibitors for mild steel, Colloids Surf. A Physicochem. Eng. Asp. 599 (2020), 124857.

[77] A. Elbarki, W. Guerrab, T. Laabaissi, F. Benhiba, Z. Rouifi, H. Qudda, A. Guenbour, R. Touir, I. Warad, Y. Ramli, A. Zarrouk, Chemical, electrochemical and theoretical studies of 3-methyl-5,5'-diphenylimidazolidine-2,4-dione as corrosion inhibitor for mild steel in HCl solution, Chem. Data Collect. 28 (2020), 100454.

[78] M. Oubaaqa, M. Ouakki, M. Rbaa, A. Abousalem, M. Maatallah, F. Benhiba, A. Jarid, M.E. Touhami, A. Zarrouk, Insight into the corrosion inhibition of new amino-acids as efficient inhibitors for mild steel in HCl solution: experimental studies, and theoretical calculations, J. Mol. Liq. 334 (2021), 116520.

[79] A.S. Fouda, M.A. Ismail, A.S. Abousalem, G.Y. Elewady, Experimental and theoretical studies on corrosion inhibition of 4-amidinophenyl-2,2'-bifuran and its analogues in acidic media, RSC Adv. 73 (2017) 45885–46528.

[80] R. Hsissou, O. Dagdaga, S. About, F. Benhiba, M. Berradi, M. El Bouchti, A. Berisha, N. Hajjaji, A. Elharfi, Novel derivative epoxy resin TGETET as a corrosion inhibition of E24 carbon steel in 1.0M HCl solution. Experimental and computational (DFT and MD simulations) methods, J. Mol. Liq. 284 (2019) 182–192.
[81] N. Wazzan, Oxaxolidine derivatives as corrosion inhibitors for API X60 steel in 1 M HCl solution: experimental and theoretical studies, Int. J. Electrochem. Sci. 14 (2019) 7450–7469.
[82] H. Lgaz, R. Salghi, K. Bhat, A. Chaouiki, S. Shubhalaxmi, S. Jodeh, Correlated experimental and theoretical study on inhibition behavior of novel quinolone derivatives for the corrosion of mild steel in hydrochloric acid solution, J. Mol. Liq. 244 (2017) 154–168.
[83] O.D. Onukwuli, V.C. Anadebe, C.S. Okafor, Optimum prediction for inhibition efficiency of Sapium ellipticum leaf extract as corrosion inhibitor of aluminum alloy (AA 3003) in hydrochloric acid solution using electrochemical impedance spectroscopy and response surface methodology, Bull. Chem. Soc. Ethiop. 34 (1) (2020) 175–191.
[84] C.S. Okafor, V.C. Anadebe, O.D. Onukwuli, Experimental, statistical modelling and molecular dynamics simulation concept of *Sapium ellipticum* leaf extract as corrosion inhibitor for carbon steel in acid environment, S. Afr. J. Chem. 72 (2019) 164–175.